

# Polytorsional-amide-induced ten helical-based coordination polymers with difunctional electrochemical activities

Guocheng Liu,<sup>a,b\*</sup> Jing Zhao,<sup>a</sup> Shuang Liang,<sup>a</sup> Yan Li,<sup>a</sup> Zhihan Chang,<sup>a</sup> Xiuli Wang<sup>a\*</sup> and Baokuan Chen<sup>c\*</sup>

<sup>a</sup> College of Chemistry and Materials Engineering, Professional Technology Innovation Center of Liaoning Province for Conversion Materials of Solar Cell, Bohai University, Jinzhou 121013, P. R. China.

<sup>b</sup> Key Laboratory of Cluster Science Ministry of Education, Beijing Key Laboratory of Photoelectronic/Electrophotonic, Advanced Research Institute of Multidisciplinary Science, School of Chemistry and Chemical Engineering, Beijing Institute of Technology, Beijing 100081, P. R. China.

<sup>c</sup> College of Chemistry, Chemical Engineering and Environmental Engineering, Liaoning Shihua University, Fushun, 113001, P. R. China.

## Materials and methods

Synthesis of the ligand **L** (*N,N'*-bis(pyridin-4-ylmethyl) naphthalene-1,4-dicarboxamide) was prepared according to a reported method<sup>[1]</sup>. All the other chemicals purchased were of reagent grade and were used without further purification. IR spectra (KBr pellets) and powder X-ray diffraction were performed with a Varian-640 spectrometer and an Ultima IV diffractometer (40 kV and 40 mA, Cu- $K\alpha$ ), respectively. The electrochemical experiment data were obtained with a CHI 760 electrochemical quartz crystal microbalance.

## X-ray crystallography

The X-ray diffraction data of the complexes **1–10** were collected by the  $\varphi$ - $\omega$  scanning technique on a Bruker SMART APEX II diffractometer equipped with a CCD area detector and a graphite monochromatic Mo- $K\alpha$  ( $\lambda = 0.71073$  Å). All structures are solved by a direct method, and anisotropic refinement is performed using SHELXS and SHELXL programs<sup>[2]</sup>. Table 1 summarizes the crystal parameters, data collection and purification results. The selected bond distances and bond angles are listed in Tables S1–S10.

## Preparation of **1–10**

**Synthesis of [Ni(L)<sub>2</sub>(2-NBA)<sub>2</sub>] (1).** A mixture containing NiCl<sub>2</sub>·6H<sub>2</sub>O (0.048 g, 0.2 mmol), **L** (0.040 g, 0.1 mmol), 2-HNBA (0.033 g, 0.2 mmol), NaOH (0.008 g, 0.20

mmol) and H<sub>2</sub>O (8 mL) was placed in a 25 mL Teflonlined autoclave and kept at 120 °C for 4 days. After slow cooling to room temperature, green crystals of **1** were obtained in 5% yield based on L. Calcd for C<sub>62</sub>H<sub>48</sub>NiN<sub>10</sub>O<sub>12</sub>: C, 62.91; H, 4.09; N, 11.83%. Found: C, 62.87; H, 4.04; N, 11.86%. IR (KBr, cm<sup>-1</sup>): 3309 m, 2911 w, 1649 s, 1604 s, 1518 s, 1430 s, 1377 s, 1348 s, 1307 s, 1249 s, 1067 m, 868 m, 839 m, 786 m, 745 m, 698 m, 640 m, 617 m.

**Synthesis of [Ni(L)(4-NBA)<sub>2</sub>(H<sub>2</sub>O)<sub>2</sub>] (2).** The synthetic method for **2** is the same as that for **1** except that 2-HNBA is replaced by 4-HNBA. Green crystals of **2** were obtained in 22% yield based on L. Calcd for C<sub>38</sub>H<sub>28</sub>NiN<sub>6</sub>O<sub>12</sub>: C, 59.70; H, 3.44; N, 10.26%. Found: C, 59.73; H, 3.46; N, 10.22%. IR (KBr, cm<sup>-1</sup>): 3390 w, 3250 w, 2945 w, 1647 s, 1617 s, 1582 s, 1524 s, 1424 s, 1389 s, 1348 s, 1015 m, 880 m, 804 s, 722 s, 628 w.

**Synthesis of [Ni(L)(PTA)<sub>2</sub>(H<sub>2</sub>O)<sub>2</sub>] (3).** The synthetic method for **3** is the same as that for **1** except that 2-HNBA is replaced by HPTA. Green crystals of **3** were obtained in 9% yield based on L. Calcd for C<sub>40</sub>H<sub>38</sub>NiN<sub>4</sub>O<sub>8</sub>: C, 63.09; H, 5.03; N, 7.36%. Found: C, 63.03; H, 5.12; N, 7.39%. IR (KBr, cm<sup>-1</sup>): 3390 w, 3250 w, 2939 w, 1641 s, 1617 s, 1582 s, 1436 s, 1389 s, 1342 s, 1260 m, 968 w, 880 w, 798 s, 722 s, 663 w, 611 m.

**Synthesis of [Ni(L)(1,2-BDC)(H<sub>2</sub>O)<sub>3</sub>]·H<sub>2</sub>O (4).** The synthetic method for **4** is the same as that for **1** except that 2-HNBA is replaced by 1,2-H<sub>2</sub>BDC (0.017 g, 0.1 mmol). Green crystals of **4** were obtained in 7% yield based on L. Calcd for C<sub>31</sub>H<sub>32</sub>NiN<sub>4</sub>O<sub>10</sub>: C, 55.60; H, 4.67; N, 8.10%. Found: C, 54.63; H, 4.72; N, 8.14%. IR (KBr, cm<sup>-1</sup>): 3402 w, 3244 w, 2922 w, 2354 w, 1641 s, 1612 s, 1533 s, 1430 s, 1395 s, 1307 m, 1266 m, 1032 w, 974 w, 769 m, 710 m, 687 m, 652 w, 611 w.

**Synthesis of [Ni(L)(PDA)]·0.5H<sub>2</sub>O (5).** The synthetic method for **5** is the same as that for **1** except that 2-HNBA is replaced by H<sub>2</sub>PDA (0.019 g, 0.1 mmol). Green crystals of **5** were obtained in 24% yield based on L. Calcd for C<sub>68</sub>H<sub>56</sub>Ni<sub>2</sub>N<sub>8</sub>O<sub>13</sub>: C, 62.32; H, 4.31; N, 8.55%. Found: C, 62.35; H, 4.32; N, 8.59%. IR (KBr, cm<sup>-1</sup>): 3291 m, 2910 w, 1641 s, 1612 s, 1535 s, 1428 s, 1401 s, 1219 m, 1026 m, 968 m, 851 w, 816 m, 775 w, 722 s, 634 w.

**Synthesis of [Ni(L)(PIM)]·0.5H<sub>2</sub>O (6).** The synthetic method for **6** is the same as that for **1** except that 2-HNBA is replaced by H<sub>2</sub>PIM (0.016 g, 0.1 mmol). Green crystals of **6** were obtained in 15% yield based on L. Calcd for C<sub>62</sub>H<sub>60</sub>Ni<sub>2</sub>N<sub>8</sub>O<sub>13</sub>: C, 59.93; H, 4.87; N, 9.02%. Found: C, 59.83; H, 4.82; N, 9.06%. IR (KBr, cm<sup>-1</sup>): 3380 w, 3238 w, 3062 w, 2928 m, 2349 w, 1653 s, 1612 s, 1547 s, 1424 s, 1301 s, 1219 m, 1073 m, 1026 m, 974 w, 851 m, 763 m, 716 w, 669 w, 605 w.

**Synthesis of [Cu(L)(4-NBA)<sub>2</sub>] (7).** A mixture containing CuCl<sub>2</sub>·2H<sub>2</sub>O (0.034 g, 0.2 mmol), **L** (0.040 g, 0.1 mmol), 4-HNBA (0.033 g, 0.2 mmol), NaOH (0.008 g, 0.2 mmol) and H<sub>2</sub>O (6 mL) was placed in a 25 mL Teflonlined autoclave and kept at 120 °C for 4 days. After slow cooling to room temperature, blue crystals of **7** were obtained in 26% yield based on L. Calcd for C<sub>38</sub>H<sub>28</sub>CuN<sub>6</sub>O<sub>10</sub>: C, 57.61; H, 3.52; N, 10.61%. Found: C, 57.74; H, 3.34; N, 10.59%. IR (KBr, cm<sup>-1</sup>): 3279 w, 2934 w, 1647 s, 1588 s, 1518 s, 1430 m, 1383 m, 1336 s, 1102 m, 1061 m, 974 w, 886 w, 827 s, 792 w, 728 s, 720 s.

**Synthesis of [Cu(L)(OMSA)<sub>2</sub>(H<sub>2</sub>O)] (8).** The synthetic method for **8** is the same as that for **7** except that HPNB is replaced by HOMSA (0.030 g, 0.2 mmol). Blue crystals of **8** were obtained in 12% yield based on L. Calcd for C<sub>40</sub>H<sub>36</sub>CuN<sub>4</sub>O<sub>9</sub>: C, 61.57; H, 4.65; N, 7.18%. Found: C, 61.46; H, 4.72; N, 7.19%. IR (KBr, cm<sup>-1</sup>): 3425 w, 2940 w, 1612 s, 1524 s, 1454 m, 1424 s, 1401 s, 1301 s, 1161 m, 968 m, 857 m, 763 s, 663 s.

**Synthesis of [Cu(L)(PRO)(H<sub>2</sub>O)]·3H<sub>2</sub>O (9).** The synthetic method for **9** is the same as that for **7** except that HPNB is replaced by H<sub>2</sub>PRO (0.010 g, 0.1 mmol). Blue crystals of **9** were obtained in 8% yield based on L. Calcd for C<sub>27</sub>H<sub>28</sub>CuN<sub>4</sub>O<sub>10</sub>: C, 51.31; H, 4.47; N, 8.86%. Found: C, 51.36; H, 4.52; N, 8.97%. IR (KBr, cm<sup>-1</sup>): 3437 w, 2910 w, 2354 m, 1658 s, 1606 s, 1547 s, 1418 s, 1377 w, 1096 s, 962 m, 851 w, 780 s, 722 w, 663 w, 617 w.

**Synthesis of [Cu(L)(AZE)(H<sub>2</sub>O)] (10).** The synthetic method for **10** is the same as that for **7** except that HPNB is replaced by H<sub>2</sub>AZE (0.019 g, 0.1 mmol). Blue crystals of **10** were obtained in 27% yield based on L. Calcd for C<sub>33</sub>H<sub>36</sub>CuN<sub>4</sub>O<sub>7</sub>: C, 59.67; H, 5.46; N, 8.44%. Found: C, 59.83; H, 5.42; N, 8.49%. IR (KBr, cm<sup>-1</sup>): 3291

m, 2934 w, 1664 s, 1617 s, 1574 s, 1541 s, 1413 s, 1295 s, 1249 s, 1208 m, 1149 w, 1038 m, 985 w, 862 m, 757 m, 716 w, 652w.

### IR and powder X-ray diffraction

The IR spectra of **1–10** are shown in the frequency range of 500–4000 cm<sup>−1</sup> (Fig. S5). The characteristic peak of the –OH group in the water molecule of **1–10** was observed in the range of approximately 3300 to 3500 cm<sup>−1</sup><sup>[3]</sup>. The absorption peak in the range of 2910 to 2945 cm<sup>−1</sup> can be attributed to the –CH<sub>2</sub> group in ligand<sup>[4]</sup>. The ν<sub>C=O</sub> vibration peak in the amide group of **L** is approximately in the range of 1600 to 1664 cm<sup>−1</sup><sup>[5]</sup>. The vibration range of naphthalene ring is within 1400–1600 cm<sup>−1</sup><sup>[6]</sup>. The peak position of the **1–10** at about 1420 cm<sup>−1</sup> is attributed to the stretching vibration of the carboxyl group<sup>[7]</sup>. In addition, the strong band in the range of 660 to 738 cm<sup>−1</sup> can be attributed to the ν<sub>C–N</sub> vibration of the N-heterocyclic rings of the **L** ligands<sup>[8]</sup>.

The phase purities of the **1–10** was examined by powder X-ray diffraction (PXRD) patterns obtained from comparative experiments. It can be seen from Fig. S6 that the experimental peak position of these complexes is almost the same as the simulated diffraction peak, which indicates that the sample is a pure phase. The slight difference between the intensity of the simulated peak and the experimental peak is due to the different orientation of the sample powder<sup>[9]</sup>.

## References

- [1] M. Sarkar and K. Biradha, *Cryst. Growth Des.*, 2006, **6**, 202.
- [2] G. M. Sheldrick, *Acta Crystallogr., Sect. A: Found. Crystallogr.*, 2008, **64**, 112.
- [3] L. N. Zhu, Z. P. Deng, S. W. Ng, L. H. Huo and S. Gao, *Dalton Trans.*, 2019, **48**, 7589.
- [4] G. H. Ni, Z. Li, Q. Sun, S. Li and K. Dong, *Adv Powder Technol*, 2019, **30**, 610.
- [5] L. Yang, F. Wang, D. Y. Auphedeous and C. L. Feng, *Nanoscale*, 2019, **11**, 14210.
- [6] C. Li, J. Xue, J. Ma and J. Li, *J. Electroanal. Chem.*, 2018, **166**, A5221.
- [7] X. L. Wang, B. Mu, H. Y. Lin and G. C. Liu, *J. Organomet. Chem.*, 2011, **696**, 2313.
- [8] B. Dolenský, R. Konvalinka, M. Jakubek and V. Král, *J. Mol. Struct.*, 2013, **1035**, 124.
- [9] X. Zhou, P. Liu, W. H. Huang, M. Kang, Y. Y. Wang and Q. Z. Shi, *CrystEngComm*, 2013, **15**, 8125.

**Table S1.** Selected bond distances ( $\text{\AA}$ ) and angles ( $^{\circ}$ ) for complex **1**

<b>1</b>			
Ni(1)–O(1)A	2.808(3)	Ni(1)–N(4)C	2.140(4)
Ni(1)–O(1)	2.808(3)	Ni(1)–N(1)	2.157(4)
Ni(1)–N(4)B	2.140(4)	Ni(1)–N(1)A	2.158(4)
O(1)A–Ni(1)–O(1)	179.998(1)	O(1)–Ni(1)–N(1)	87.76(13)
O(1)A–Ni(1)–N(4)B	86.86(13)	N(4)B–Ni(1)–N(1)	84.97(14)
O(1)–Ni(1)–N(4)B	93.15(13)	N(4)C–Ni(1)–N(1)	95.03(14)
O(1)A–Ni(1)–N(4)C	93.15(13)	O(1)A–Ni(1)–N(1)A	87.76(13)
O(1)–Ni(1)–N(4)C	86.85(13)	O(1)–Ni(1)–N(1)A	92.24(13)
N(1)B–Ni(1)–N(4)C	180	N(1)B–Ni(1)–N(1)A	93.03(14)
O(1)A–Ni(1)–N(1)	92.24(13)	N(1)C–Ni(1)–N(1)A	84.96(14)
N(1)–Ni(1)–N(1)A	180		

A:  $-x + 1, -y, -z + 1$ ; B:  $x + 1, -y + 1/2, z - 1/2$ ; C:  $-x + 1, y - 1/2, -z + 3/2$ **Table S2.** Selected bond distances ( $\text{\AA}$ ) and angles ( $^{\circ}$ ) for complex **2**

<b>2</b>			
Ni(1)–O(1)A	2.018(4)	Ni(1)–O(2)	2.079(5)
Ni(1)–O(1)	2.018(4)	Ni(1)–N(1)	2.107(6)
Ni(1)–O(2)A	2.079(5)	Ni(1)–N(1)A	2.107(6)
O(1)A–Ni(1)–O(1)	180	O(1)–Ni(1)–O(2)A	88.2(2)
O(1)A–Ni(1)–O(2)A	91.8(2)	O(1)A–Ni(1)–O(2)	88.2(2)
O(1)–Ni(1)–O(2)	91.8(2)	O(1)A–Ni(1)–N(1)A	87.4(2)
O(2)A–Ni(1)–O(2)	179.998(1)	O(1)–Ni(1)–N(1)A	92.6(2)
O(1)A–Ni(1)–N(1)	92.6(2)	O(2)A–Ni(1)–N(1)	89.3(2)
O(1)–Ni(1)–N(1)	87.4(2)	O(2)–Ni(1)–N(1)	90.7(2)
O(2)A–Ni(1)–N(1)	90.7(2)	N(1)–Ni(1)–N(1)A	179.998(1)
O(2)–Ni(1)–N(1)	89.3(2)		

A:  $-x + 1/2, -y + 1/2, -z + 1$

**Table S3.** Selected bond distances ( $\text{\AA}$ ) and angles ( $^{\circ}$ ) for complex **3**

3			
Ni(1)–O(1W)	2.075(4)	Ni(1)–O(2)A	2.006(3)
Ni(1)–O(1W)A	2.075(4)	Ni(1)–N(1)	2.116(5)
Ni(1)–O(2)	2.006(3)	Ni(1)–N(1)A	2.116(5)
O(2)A–Ni(1)–O(2)	179.999(1)	O(2)A–Ni(1)–N(1)A	92.28(16)
O(2)A–Ni(1)–O(1W)	91.49(16)	O(2)–Ni(1)–N(1)A	87.72(16)
O(2)–Ni(1)–O(1W)	88.52(16)	O(1W)–Ni(1)–N(1)A	92.97(17)
O(2)–Ni(1)–O(1W)A	91.48(16)	O(2)A–Ni(1)–N(1)	87.72(16)
O(1W)–Ni(1)–O(1W)A	179.998(1)	O(2)–Ni(1)–N(1)	92.28(16)
O(1W)–Ni(1)–N(1)	87.03(17)	O(1W)A–Ni(1)–N(1)	92.98(17)
N(1)A–Ni(1)–N(1)	180.0	O(2)A–Ni(1)–O(1W)A	88.52(16)
O(1W)A–Ni(1)–N(1)A	87.03(17)		
A: $-x + 1/2, -y + 1/2, -z + 1$			

**Table S4.** Selected bond distances ( $\text{\AA}$ ) and angles ( $^{\circ}$ ) for complex **4**

4			
Ni(1)–O(3)	2.0497(15)	Ni(1)–N(1)	2.089(2)
Ni(1)–O(3W)	2.0640(17)	Ni(1)–N(4)A	2.0917(19)
Ni(1)–O(2W)	2.0812(16)	Ni(1)–O(1W)	2.1050(17)
O(3)–Ni(1)–O(3W)	89.45(7)	O(2W)–Ni(1)–N(4)A	93.98(7)
O(3)–Ni(1)–O(2W)	90.52(6)	N(1)–Ni(1)–N(4)A	90.09(8)
O(3W)–Ni(1)–O(2W)	93.57(7)	O(3)–Ni(1)–O(1W)	80.74(6)
O(3)–Ni(1)–N(1)	89.87(7)	O(3W)–Ni(1)–O(1W)	86.83(7)
O(3W)–Ni(1)–N(1)	177.38(8)	O(2W)–Ni(1)–O(1W)	171.25(6)
O(2W)–Ni(1)–N(1)	88.97(7)	N(1)–Ni(1)–O(1W)	90.56(7)
O(3)–Ni(1)–N(4)A	175.51(7)	N(4)A–Ni(1)–O(1W)	94.77(7)
O(3W)–Ni(1)–N(4)A	90.38(7)		
A: $x - 1, y + 1, z$			

**Table S5.** Selected bond distances ( $\text{\AA}$ ) and angles ( $^{\circ}$ ) for complex **5**

5			
Ni(1)–O(6)	2.0388(18)	Ni(1)–O(3)B	2.0898(19)
Ni(1)–N(4)	2.054(2)	Ni(1)–O(4)B	2.1477(19)
Ni(1)–N(2)A	2.069(2)	Ni(1)–O(5)	2.2086(18)
O(6)–Ni(1)–N(4)	97.56(8)	N(2)–Ni(1)–O(4)B	93.12(8)
O(6)–Ni(1)–N(2)A	96.87(8)	O(3)B–Ni(1)–O(4)B	61.96(7)
N(4)–Ni(1)–N(2)A	94.55(9)	O(6)–Ni(1)–O(5)	61.87(7)
O(6)–Ni(1)–O(3)B	159.09(8)	N(4)–Ni(1)–O(5)	91.60(8)
N(4)–Ni(1)–O(3)B	97.11(8)	N(2)A–Ni(1)–O(5)	158.51(8)
N(2)A–Ni(1)–O(3)B	96.73(8)	O(3)B–Ni(1)–O(5)	102.93(8)
O(6)A–Ni(1)–O(4)B	101.47(7)	O(4)B–Ni(1)–O(5)	88.56(7)
N(4)–Ni(1)–O(4)B	158.45(8)		
A: $x + 1/2, y - 1, z$ ; B: $x, y + 1, z$			

**Table S6.** Selected bond distances ( $\text{\AA}$ ) and angles ( $^{\circ}$ ) for complex **6**

6			
Ni(3)–O(2)	2.0388(18)	Ni(1)–O(3)B	2.0898(19)
Ni(1)–N(1)	2.054(2)	Ni(1)–O(4)B	2.1477(19)
Ni(1)–N(4)A	2.069(2)	Ni(1)–O(1)	2.2086(18)
O(2)–Ni(1)–N(1)	97.56(8)	N(4)–Ni(1)–O(4)B	93.12(8)
O(2)–Ni(1)–N(4)A	96.87(8)	O(3)B–Ni(1)–O(4)B	61.96(7)
N(1)–Ni(1)–N(4)A	94.55(9)	O(2)–Ni(1)–O(1)	61.87(7)
O(2)–Ni(1)–O(3)B	159.09(8)	N(1)–Ni(1)–O(1)	91.60(8)
N(1)–Ni(1)–O(3)B	97.11(8)	N(4)A–Ni(1)–O(1)	158.51(8)
N(4)A–Ni(1)–O(3)B	96.73(8)	O(3)B–Ni(1)–O(1)	102.93(8)
O(2)A–Ni(1)–O(4)B	101.47(7)	O(4)B–Ni(1)–O(1)	88.56(7)
N(1)–Ni(1)–O(4)B	158.45(8)		
A: $x + 1/2, y - 1, z$ ; B: $x, y + 1, z$			

**Table S7.** Selected bond distances ( $\text{\AA}$ ) and angles ( $^\circ$ ) for complex **7**

7			
Cu(1)–O(1)	1.913(3)	Cu(1)–N(1)	2.011(4)
Cu(1)–O(2)	1.925(7)	Cu(1)–N(4)A	2.024(4)
O(1)–Cu(1)–O(2)	175.44(16)	O(1)–Cu(1)–N(4)A	90.75(15)
O(1)–Cu(1)–N(1)	90.33(15)	O(2)–Cu(1)–N(4)A	87.76(15)
O(2)–Cu(1)–N(1)	90.00(15)	N(1)–Cu(1)–N(4)A	165.11(16)
A: $-x, y - 1, -z + 3/2$			

**Table S8.** Selected bond distances ( $\text{\AA}$ ) and angles ( $^\circ$ ) for complex **8**

8			
Cu(1)–O(6)	1.932(5)	Cu(1)–N(1)	2.019(6)
Cu(1)–O(3)	1.944(6)	Cu(1)–N(4)A	2.038(6)
Cu(1)–O1W	2.471(7)		
O(6)–Cu(1)–O(3)	173.2(2)	O(6)–Cu(1)–N(1)	90.4(2)
O(3)–Cu(1)–N(1)	85.4(2)	O(6)–Cu(1)–N(4)A	93.1(2)
O(3)–Cu(1)–N(4)A	90.6(2)	N(1)–Cu(1)–N(4)A	173.8(3)
O(6)–Cu(1)–O(1W)	84.0(2)	O(3)–Cu(1)–O(1W)	101.8(3)
N(1)–Cu(1)–O(1W)	97.0(3)	N(4)A–Cu(1)–O(1W)	88.4(2)
A: $x + 1, y, z - 1$			

**Table S9.** Selected bond distances ( $\text{\AA}$ ) and angles ( $^{\circ}$ ) for complex **9**

<b>9</b>			
Cu(1)–O(1W)	2.305(3)	Cu(1)–N(1)	2.013(3)
Cu(1)–O(1)	1.919(3)	Cu(1)–N(4)A	2.016(3)
Cu(1)–O(2)	1.929(3)		
O(1W)–Cu(1)–O(1)	95.29(13)	O(1W)–Cu(1)–N(4)A	97.48(13)
O(1W)–Cu(1)–N(1)	96.30(1)	O(1)–Cu(1)–N(4)A	167.18(15)
O(1)–Cu(1)–N(1)	89.10(13)	N(1)–Cu(1)–N(4)A	90.69(13)
O(2)–Cu(1)–N(4)A	86.01(13)	O(2)–Cu(1)–N(1)	170.18(14)
O(2)–Cu(1)–O(1W)	93.30(12)	O(2)–Cu(1)–O(1)	92.07(12)
A: $x, -y + 3/2, z - 1/2$			

**Table S10.** Selected bond distances ( $\text{\AA}$ ) and angles ( $^{\circ}$ ) for complex **10**

<b>10</b>			
Cu(1)–O(1)	1.954(3)	Cu(1)–N(4)B	2.026(3)
Cu(1)–O(4)A	1.998(3)	Cu(1)–O(1W)	2.232(3)
Cu(1)–N(1)	2.013(3)		
O(1)–Cu(1)–O(4)A	164.28(11)	O(4)A–Cu(1)–O(1W)	95.45(11)
O(1)–Cu(1)–N(1)	87.74(13)	O(1)–Cu(1)–O(1W)	100.22(12)
O(4)A–Cu(1)–N(1)	93.26(13)	N(4)B–Cu(1)–O(1W)	95.97(12)
O(1)–Cu(1)–N(4)B	88.50(14)	O(1W)–Cu(1)–N(1)	91.29(13)
O(4)A–Cu(1)–N(4)B	88.56(13)	N(1)–Cu(1)–O(1W)	91.22(12)
N(1)–Cu(1)–N(4)B	172.39(13)		
A: $x - 1, y, z$ ; B: $x - 1, y + 1, z - 1$			

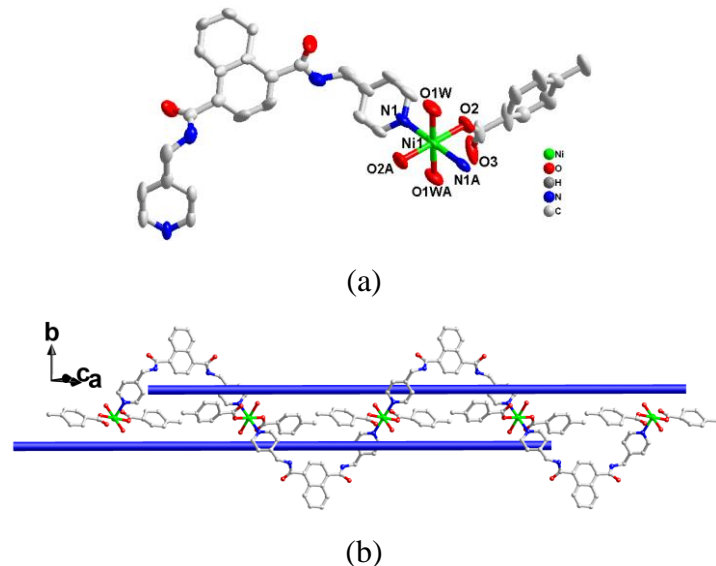


**Fig. S1** (a) The coordination environment of  $\text{Ni}^{2+}$  in **3**. (b) 1D racemic chain.

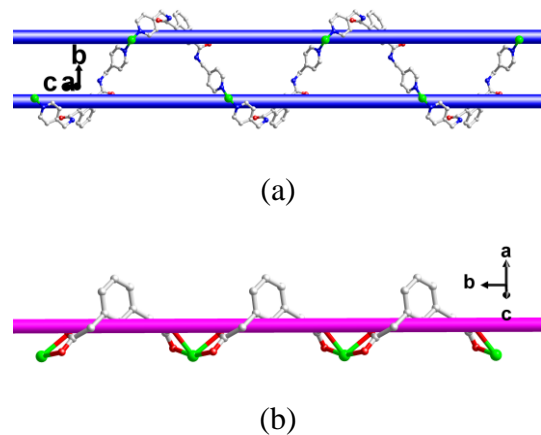
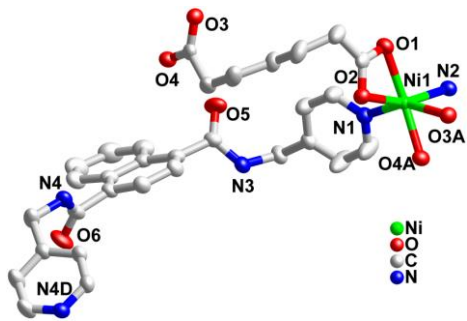
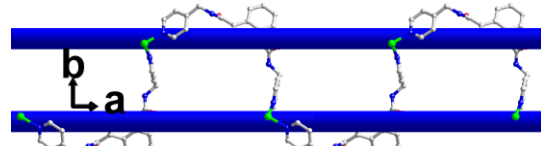


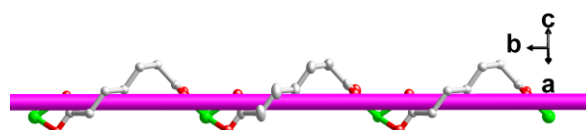
**Fig. S2** (a) 1D  $[\text{Ni}-\text{L}]_n$  racemic chain. (b) 1D  $[\text{Ni}-(\text{PDA})]_n$  spiral chain.



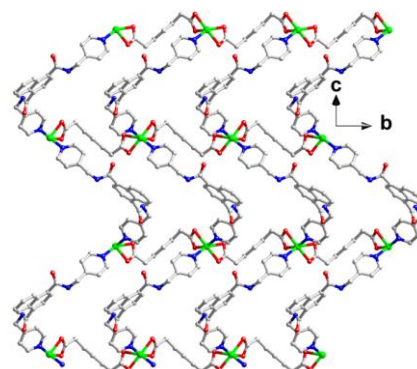
(a)



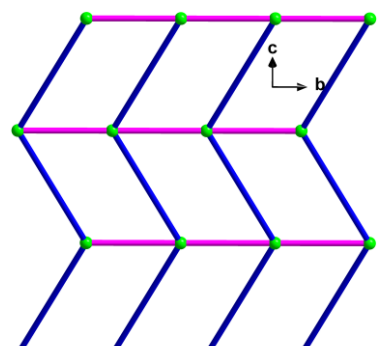
(b)



(c)

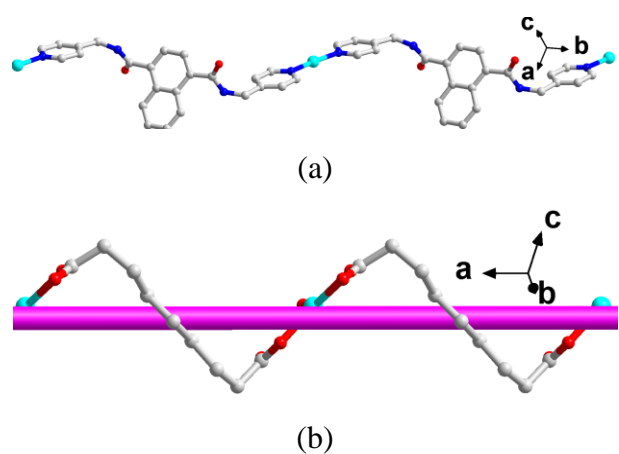


(d)

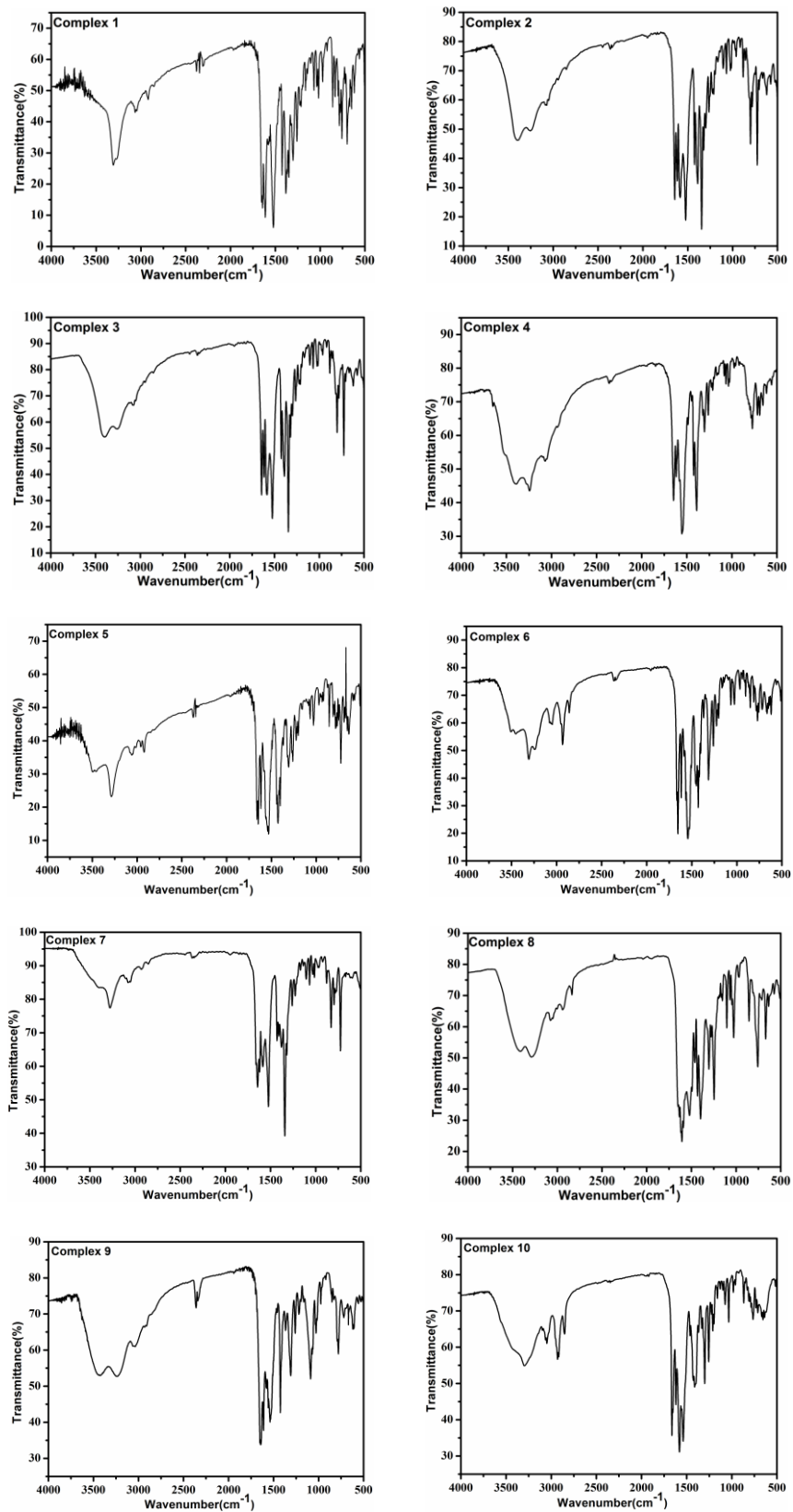


(e)

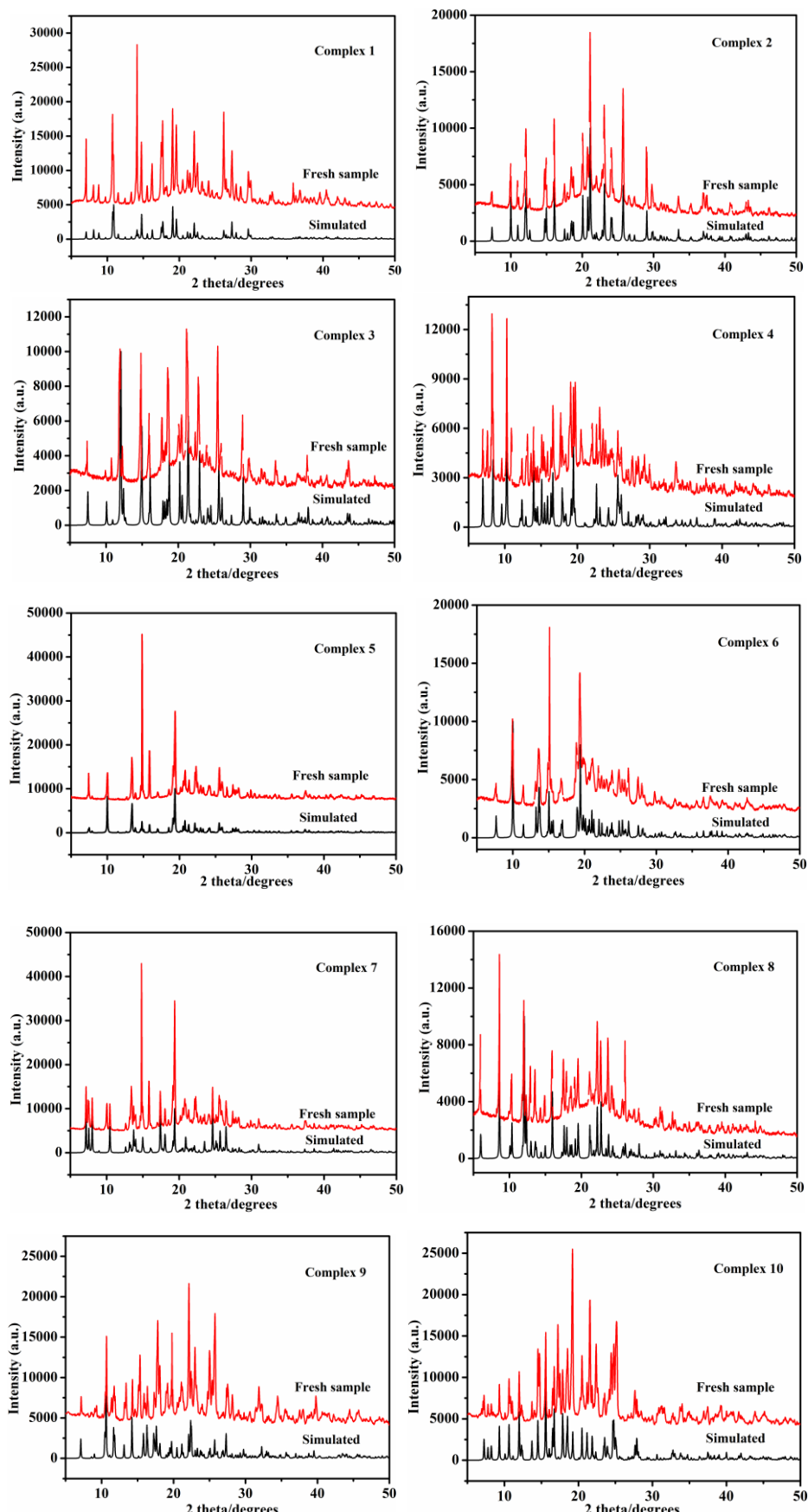
**Fig. S3** (a) The coordination environment of  $\text{Ni}^{2+}$  in **6**. (b) 1D  $[\text{Ni}-\mathbf{L}]_n$  chain. (c) 1D  $[\text{Ni}-(\text{PIM})]_n$  chain. (d) 2D layer. (e) 4-connected topology.



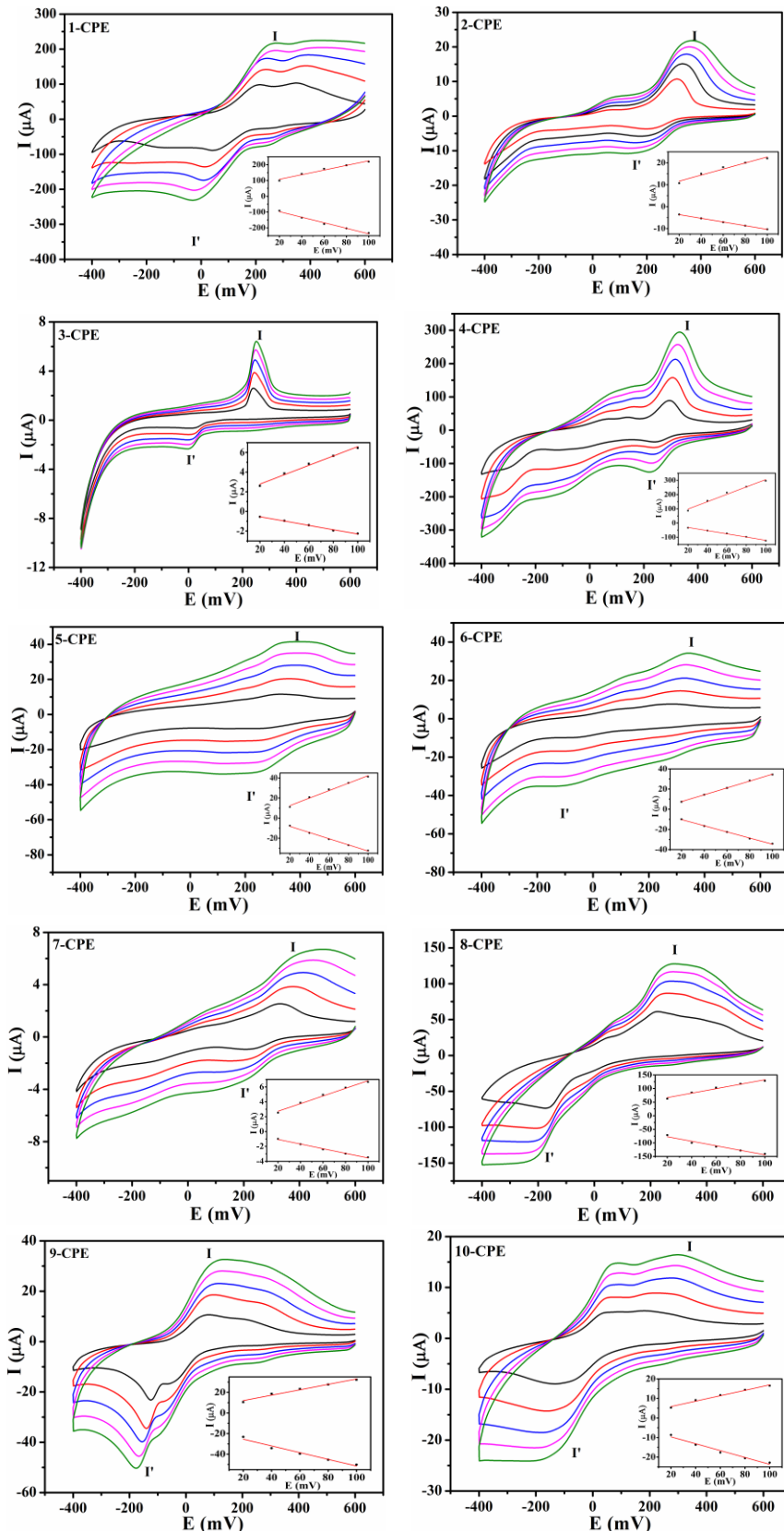
**Fig. S4** (a) 1D  $[\text{Cu}-\mathbf{L}]_n$  chain; (b) 1D  $[\text{Cu}-\text{AZE}]_n$  chain.



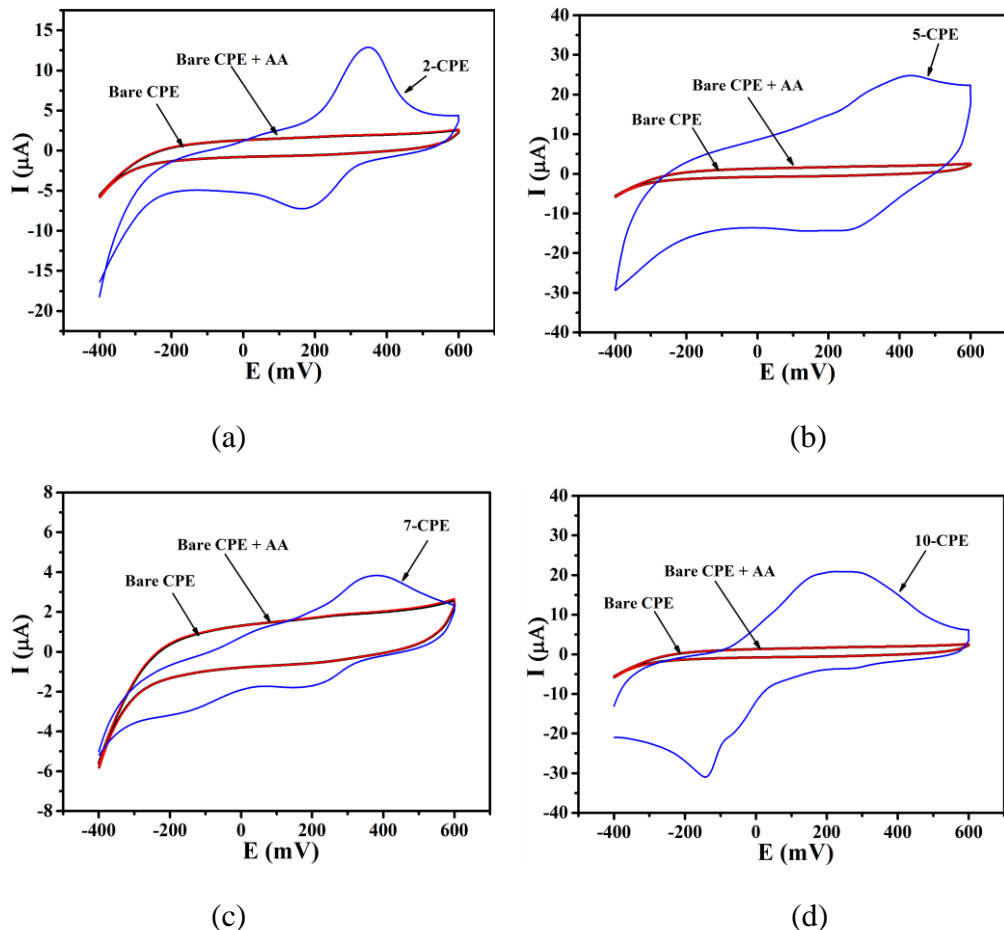
**Fig. S5** The IR spectra of **1–10**.



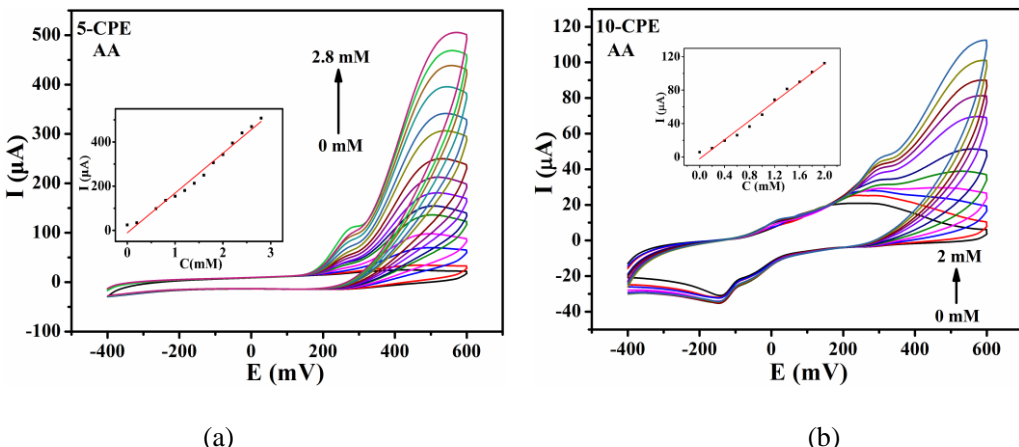
**Fig. S6** The PXRD patterns of simulated and fresh samples for **1–10**.



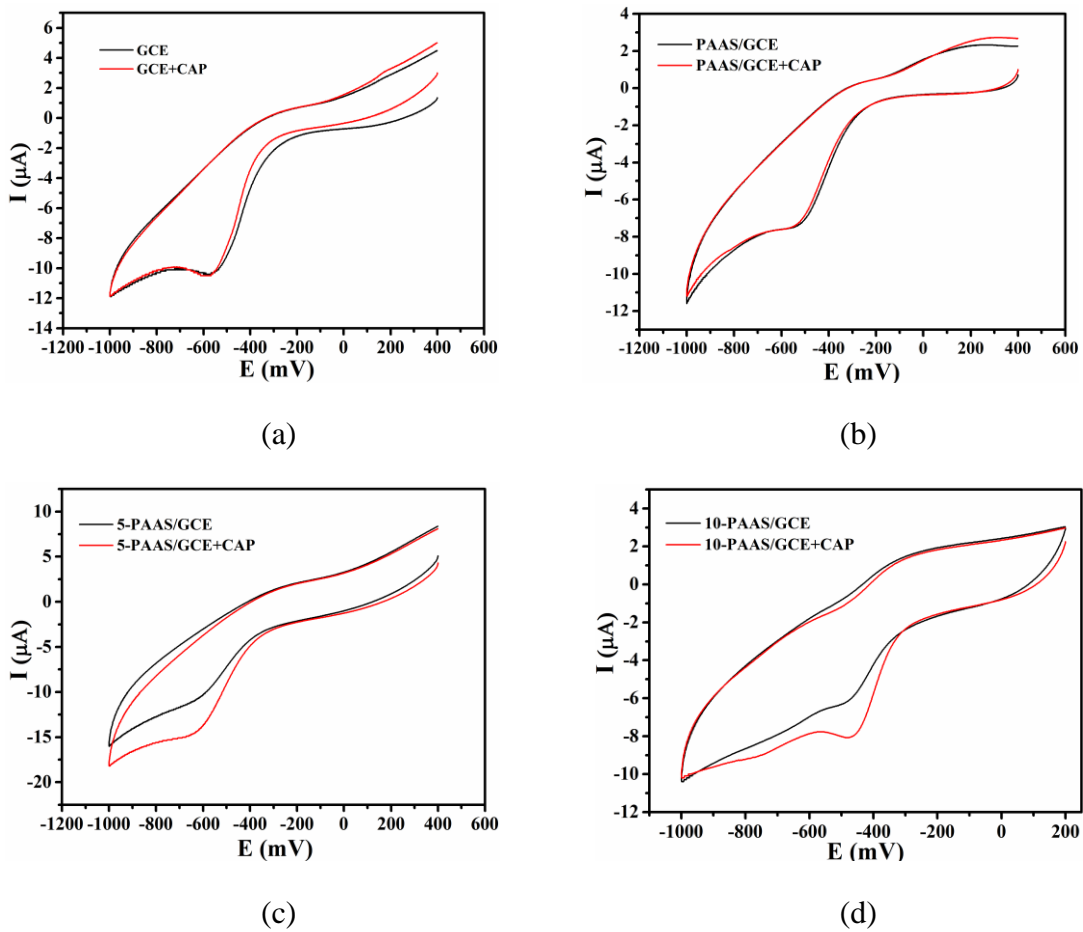
**Fig. S7** Cyclic voltammograms of the **1-CPE–10-CPE** (from inner to outer: 20, 40, 60, 80, 100, 120, 140  $\text{mV s}^{-1}$ ). Insert: the dependence of cathodic peak and anodic peak currents on scan rates of **1-CPE–10-CPE**.



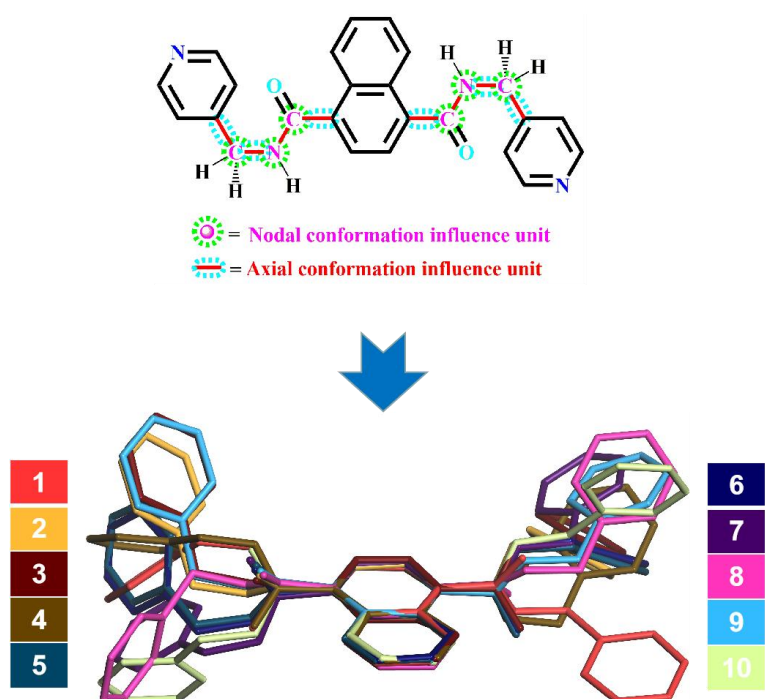
**Fig. S8** Cyclic voltammograms of bare CPE, bare CPE+AA and **2**-CPE (a), **5**-CPE (b), **7**-CPE (c) and **10**-CPE (d) in 0.01 M  $\text{H}_2\text{SO}_4$  + 0.5 M  $\text{Na}_2\text{SO}_4$  solution.



**Fig. S9** (a-b) Cyclic voltammograms of **5**, **10**-CPE at different concentrations. Scan rate:  $40 \text{ mV s}^{-1}$ .



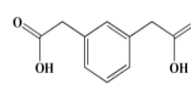
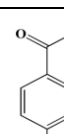
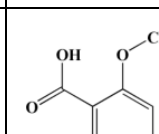
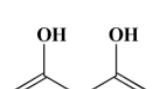
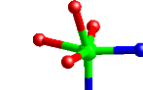
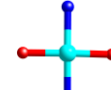
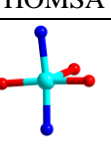
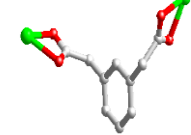
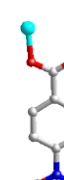
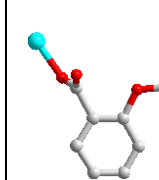
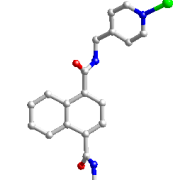
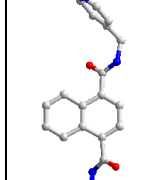
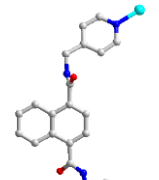
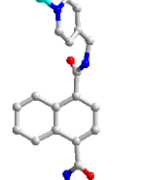
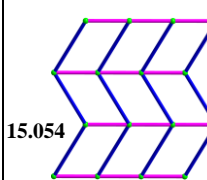
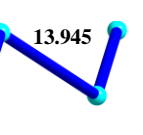
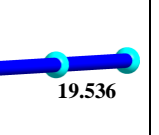
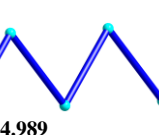
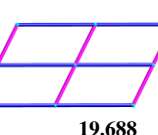
**Fig. S10** Cyclic voltammograms of bare electrode (a), PAAS/GCE (b), **5**-PAAS/GCE (c) and **10**-PAAS/GCE (d) in  $0.01 \text{ M H}_2\text{SO}_4 + 0.5 \text{ M Na}_2\text{SO}_4$  solution and  $0.01 \text{ M H}_2\text{SO}_4 + 0.5 \text{ M Na}_2\text{SO}_4$  solution containing CAP.



**Chart S1** The polytorsional features of **L** in the ten CPs with the overlay modes showing the different extending directions of pyridine groups. The figure is obtained by Materials Studio based on the CIF files of CPs **1–10**.

	<b>1</b>	<b>2</b>	<b>3</b>	<b>4</b>	<b>5</b>
(a)	 2-HNBA	 HPNB	 HPTA	 1,2-H <sub>2</sub> BDC	 H <sub>2</sub> PIM
(b)	 <i>trans</i> octahedron	 <i>trans</i> octahedron	 <i>trans</i> octahedron	 <i>cis</i> octahedron	 <i>cis</i> octahedron
(c)					
(d)					
(e)	 18.591	 14.628	 14.564	 15.976	 15.066

**Chart S2** The structural details of complexes **1–5**. (a) The carboxylic acids; (b) The coordination modes of Ni<sup>2+</sup>; (c) The subunits of Ni-carboxylates; (d) The subunits of Ni-**L**; (e) The schematic view of the structures.

	<b>6</b>	<b>7</b>	<b>8</b>	<b>9</b>	<b>10</b>
(a)	 5-H <sub>2</sub> MIP	 HPNB	 HOMSA	 H <sub>2</sub> PRO	 H <sub>2</sub> AZE
(b)	 <i>cis</i> octahedron	 <i>trans</i> square planar	 <i>trans</i> triangular bipyramid	 <i>cis</i> triangular bipyramid	 <i>trans</i> triangular bipyramid
(c)					
(d)					
(e)	 15.054	 13.945	 19.536	 14.989	 19.688

**Chart S3** The structural details of complexes **6–10**. (a) The carboxylic acids; (b) The coordination modes of M (Ni/Cu); (c) The subunits of M-carboxylates; (d) The subunits of M-L; (e) The schematic view of the structures.